Multi-resolution Probabilistic Ocean Physics-Acoustics Modeling: Validation in the New Jersey Continental Shelf

P. F. J. Lermusiaux[a,†], P. J. Haley, Jr.[a], C. Mirabito[a], W. H. Ali[a], M. Bhabra[a],
P. Abbot[b], C.-S. Chiu[b], C. Emerson[b]
[a] *Department of Mechanical Engineering, Massachusetts Institute of Technology, Cambridge, MA*
[b] *OASISLEX, Lexington, MA*
[†]Corresponding Author: pierrel@mit.edu

***Abstract*—The reliability of sonar systems in the littoral environment is greatly affected by the variability of the surrounding nonlinear ocean dynamics. This variability occurs on multiple scales in space and time, and involves multiple interacting processes, from internal tides and waves to meandering fronts, eddies, boundary layers, and strong air-sea interactions. We utilize our high-resolution MSEAS-PE ocean modeling system to hindcast the ocean physical environment off the New Jersey continental shelf for the end of June 2009, and then utilize our new MSEAS probabilistic acoustic NAPE and WAPE solvers in a coupled ocean physics-acoustic modeling fashion to predict the transmission and integrated transmission losses, respectively. The coupled models are described, and their predictions verified against independent ocean physics observations and sound propagation measurements from acoustic sources and receivers in the region. Our high-resolution ocean simulations are shown to substantial reduce the RMSE and bias of the coarser simulations. Our acoustic simulations of deterministic and stochastic TL fields also show significant skill.**

***Index Terms*—ocean modeling, acoustics modeling, transmission loss, New Jersey continental shelf**

Global Oceans 2020: Singapore - U.S. Gulf Coast | 978-1-7281-5446-6/20/$31.00 ©2020 IEEE | DOI: 10.1109/IEEECONF38699.2020.9389193

I. Introduction

The littoral environment is especially demanding on tactical sonar systems, in large part because of the spatial and temporal variability of the highly-dynamic nonlinear ocean fields. The variability occurs on multiple scales in space and time, and involves multiple interacting processes, from internal tides and waves to meandering fronts, eddies, boundary layers, and strong air-sea interactions [1]–[5]. The present goal is to improve detection rates through improved multi-resolution ocean modeling and probabilistic forecasting of littoral ocean variability relevant for underwater propagation. The acoustic emphasis is on transmission loss (TL) variability and on detection performance with 50 to 3000 Hz active signals. To exemplify the multi-resolution probabilistic modeling, we reconstruct the acoustic environment off the New Jersey continental shelf for the end of June 2009 (MAC DG-3 Test), modeling the ocean spatial-temporal variability and its impact on the transmission loss (TL) and detection performance. We utilize ocean and acoustic measurements to validate results.

The effort is part of the Surface Dynamic Uncertainty Characterization and Transfer (S-DUCT) program that aims to address some of these challenges. The goals of S-DUCT on the long-term are to (i) employ and develop our high-resolution MSEAS modeling system in ocean regimes with surface ducts to provide high-fidelity sound speed fields for acoustic studies, and (ii) quantify the sound speed and transmission loss variability in surface duct regions (e.g. mixed-layer depth variations, internal wave effects scattering acoustic energy out of the surface duct, etc.) and investigate models of such effects that are useful for naval applications.

The remainder of this paper is organized as follows. In Sect. II, we describe our methodology and systems, and specifically our MIT MSEAS-PE and MSEAS-ParEq modeling softwares and their setup for the present work. Next, in Sect. III, we show and discuss our results, which include 1 km-resolution ocean scenario simulations around June 30, 2009. We also discuss our predictions of Transmission Loss (TL) using our acoustic deterministic and stochastic MSEAS-ParEq solver, as well as skill comparison of integrated Transmission Loss (iTL) predictions against measurements. Finally, some concluding remarks are made and possible future research directions are discussed in Sect. IV.

II. Simulations Setup

A. MSEAS Ocean Physics Modeling System

For the ocean modeling hindcasts, we utilized our multi-resolution MIT-MSEAS ocean modeling system [6]–[8]. The MSEAS software is used for fundamental research and for realistic simulations and predictions in varied regions of the world's ocean [9]–[19], including monitoring [20], ecosystem prediction and environmental management [21], [22], and, importantly for the present project, oceanographic-acoustic predictions and coupled ocean-acoustic data assimilation [2], [14], [23]–[26]. For this work, we mainly employed our MIT-MSEAS hydrostatic PE code with a nonlinear free surface, based on second-order structured finite volumes [6].

The MSEAS modeling system was set up in the following manner. The computational domain shown in Fig. 1 overlaid on bathymetry, encompasses the northeast U.S. continental shelf, the shelf break and Hudson Canyon, and the northwest Sargasso Sea. It has 1 km horizontal resolution where the acoustic data were collected and is discretized using 100 optimized vertical levels. The bathymetry used merges several data sets including the 3 arc-second National Centers for Environmental Information (NCEI) U.S. Coastal Relief Model [27] and the 15 arc-second Smith and Sandwell data.

The ocean simulations are forced by atmospheric flux fields forecast by the 32 km hourly North American Model (NAM) from the National Centers for Environmental Prediction

978-1-7281-5446-6/20/$31.00 ©2020 IEEE

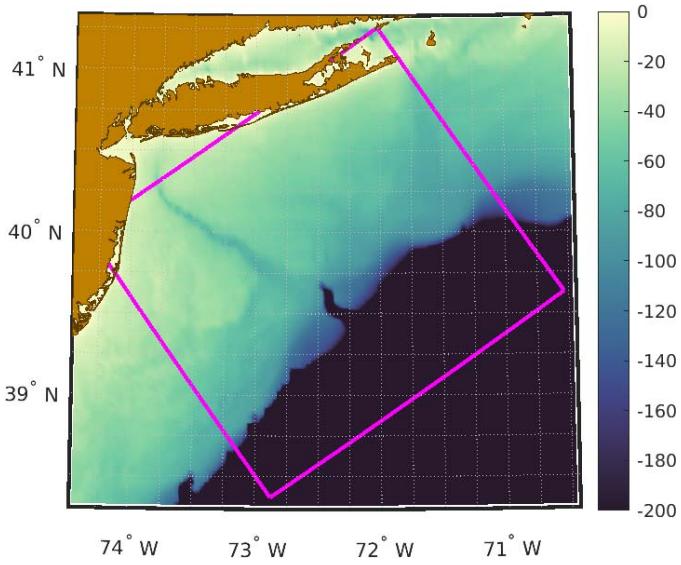

Fig. 1. MSEAS-PE 1 km modeling domain (boundary shown in magenta) over bathymetry (m).

(NCEP) [28]. During the end of June and start of July 2009, winds were relatively calm. Minor wind events, with maximum wind stresses of approximately 1 dyne/cm^2, occurred from June 26 12Z to June 27 6Z, on June 29 18Z, on June 30 18Z, on July 1 06-18Z, and on July 3 00Z-06Z. Tidal forcing from the TPXO8 model [29], [30] from Oregon State University was used, but updated for our high-resolution bathymetry, coastlines, and quadratic bottom drag.

B. Synoptic Ocean Physics Data

We collected independent synoptic data of opportunity for the period surrounding June 30, 2009, for use as inputs for initial conditions, parametrizations, and data assimilation, or for validation. The different types of these data sets are described in Fig. 2. Such data of opportunity are commonly available in real-time and usable for ocean forecasting. In addition, the OASIS XBT data from the actual sea test (MAC DG-3 Test) was employed as independent validation data.

Data	Variables	Duration
OASIS XBT	T	2009-06-30
GTSPP	T, S	2009-06-22 to 2009-07-07
NDBC Buoys	T	2009-06-22 to 2009-07-07
Satellite SST	SST	2009-06-29 10:30Z to 2009-06-30 21:26Z
WOD XBT	T	2009-06-22 00:01Z to 2009-07-06 14:35Z

Fig. 2. Available data used as model input or validation. The OASIS data is listed in the upper block, while the lower block contains the data of opportunity.

All profile data locations (by type) available between June 22 and July 7, 2009, are displayed in Fig. 3.

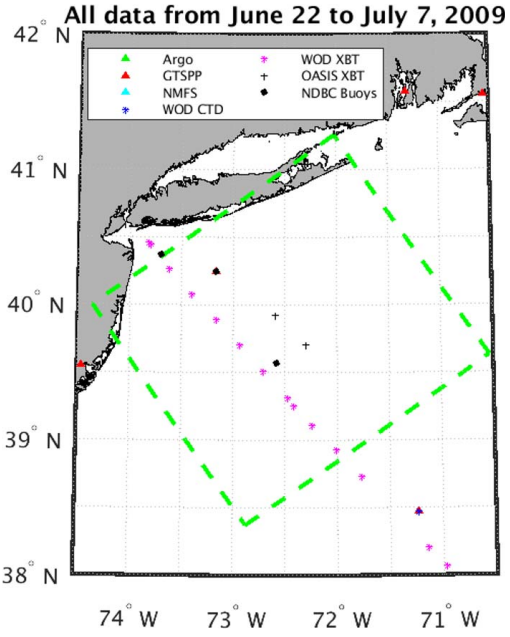

Fig. 3. Locations of data profiles (by type) between June 22 and July 7, 2009. The MSEAS-PE domain boundary is shown in green dashed lines.

C. MSEAS Ocean Acoustic Propagation Modeling

For modeling the acoustic propagation in the region of interest, we utilize our MIT-MSEAS acoustic modeling system, in the present case, the MSEAS Parabolic Equation (MSEAS-ParEq) code. The code employs the simulations of the MSEAS-PE modeling system to set up the ocean acoustic environment and implements a finite-volume discretization of the Wide-Angle acoustic Parabolic Equation (WAPE), a widely used modeling technique in underwater acoustics [31]–[33]. The WAPE can be derived from the acoustic wave equation as follows.

Assuming an isotropic broadband point source with signal strength $S(t)$, the acoustic wave equation [34] can be written as,

$$\rho\nabla\cdot\left(\frac{1}{\rho}\nabla p_t\right)-\frac{1}{c^2}\frac{\partial^2 p_t}{\partial t^2}=-S(t)\,\frac{2\delta(\boldsymbol{x}_\perp-\boldsymbol{x}_{\perp s})\,\delta(\eta)}{\eta}\,, \quad (1)$$

where ρ corresponds to the medium density, p_t is the time-domain acoustic pressure field, and c is the medium sound speed. The domain of propagation is described by Cartesian coordinates where the position $\boldsymbol{x}\in\mathcal{D}\times[0,R]$ is written as $\boldsymbol{x}=(\boldsymbol{x}_\perp,\eta)$, with $\boldsymbol{x}_\perp\in\mathcal{D}$ denoting the two-dimensional transverse coordinates, and $\eta\in[0,R]$ denoting the position in the range direction. Finally, the isotropic time-harmonic point sound source is located at $\eta=0$ and $\boldsymbol{x}_\perp=\boldsymbol{x}_{\perp,s}$.
Defining the time-frequency Fourier Transform pair as

$$\begin{aligned}\mathcal{F}\{\cdot\}&=\int_{-\infty}^{+\infty}\cdot\quad e^{i\omega t}dt,\\ \mathcal{F}^{-1}\{\cdot\}&=\frac{1}{2\pi}\int_{-\infty}^{+\infty}\cdot\quad e^{-i\omega t}d\omega\,,\end{aligned} \quad (2)$$

and working in the frequency domain, the acoustic wave equation (1) reduces to [34],

$$\rho\nabla\cdot\left(\frac{1}{\rho}\nabla P\right)+k_a^2\left(\omega\right)P=-\hat{S}\left(\omega\right)\frac{2\delta\left(\boldsymbol{x}_\perp-\boldsymbol{x}_{\perp,s}\right)\delta\left(\eta\right)}{\eta}\,, \tag{3}$$

where $P\left(\boldsymbol{x}_\perp,\eta,\omega\right)=\mathcal{F}\left\{p_t\right\}$ and the source spectrum $\hat{S}\left(\omega\right)=\mathcal{F}\left\{S\right\}$. Furthermore, $k_a\left(\omega\right)=\frac{\omega}{c}\left(1+ia\right)$ is the complex (accounting for medium absorption) wave number, $c=c\left(\boldsymbol{x}_\perp,\eta\right)$ is the space-varying medium sound speed, and $a=a\left(\boldsymbol{x}_\perp,\eta,\omega\right)$ is the attenuation coefficient.

Normalizing the pressure response by the source spectrum $p\left(\omega\right)=P\left(\omega\right)/\hat{S}\left(\omega\right)$, equation (3) reduces to the Helmholtz equation:

$$\rho\nabla\cdot\left(\frac{1}{\rho}\nabla p\right)+k_a^2\left(\omega\right)p=-\frac{2\delta\left(\boldsymbol{x}_\perp-\boldsymbol{x}_{\perp,s}\right)\delta\left(\eta\right)}{\eta}\,. \tag{4}$$

We are commonly interested in solving equation (4) for a time-harmonic source with frequency ω_0 to compute the transmission loss (TL) field

$$TL\left(\boldsymbol{x}_\perp,\eta;\omega_0\right)=-20\log\left|\frac{p\left(\boldsymbol{x}_\perp,\eta;\omega_0\right)}{p_0\left(\eta=1;\omega_0\right)}\right|\,, \tag{5}$$

where $p_0\left(\eta=1\right)$ is a nominal pressure value [32]. Yet, solving this elliptic Partial Differential Equation (PDE) in large domains of propagation is computationally expensive. To address this challenge, the Parabolic Equation (PE) technique, introduced by Tappert in [35], has been widely used [36].

Under the parabolic equation (PE) approximation [35], [37], the acoustic pressure $p\left(\boldsymbol{x}_\perp,\eta;\omega_0\right)=p\left(\boldsymbol{x}_\perp,\eta\right)$ is decomposed as

$$p\left(\boldsymbol{x}_\perp,\eta\right)=v\left(\eta\right)\psi\left(\boldsymbol{x}_\perp,\eta\right)\,, \tag{6}$$

where the functions $v\left(\eta\right)$ (strongly dependent on the range direction η) and $\psi\left(\boldsymbol{x}_\perp,\eta\right)$ (denoting the envelope of outgoing complex acoustic field) can be found to satisfy [32],

$$\begin{aligned}&v\left(\eta\right)\sim\exp\left(ik_0\eta\right),\\&\frac{\partial}{\partial\eta}\psi\left(\boldsymbol{x}_\perp,\eta\right)=ik_0\left\{\sqrt{\mathbf{I}+\mathbf{Q}}-\mathbf{I}\right\}\psi\left(\boldsymbol{x}_\perp,\eta\right)\,,\end{aligned} \tag{7}$$

where $k_0=\omega_0/c_{ref}$, with c_{ref} a reference sound speed. In addition, $\mathbf{I}$ is the identity operator, and

$$\mathbf{Q}=\left(n_a^2-1\right)\mathbf{I}+\frac{1}{k_0^2}\rho\nabla_\perp\cdot\left(\frac{1}{\rho}\nabla_\perp\right)\,, \tag{8}$$

where n_a is the index of refraction defined as,

$$n_a^2\left(\boldsymbol{x}_\perp,\eta\right)=\left(\frac{c_{ref}}{c\left(\boldsymbol{x}_\perp,\eta\right)}\right)^2\left(1+i\frac{a\left(\boldsymbol{x}_\perp,\eta\right)}{27.29}\right)\,, \tag{9}$$

and $\rho\nabla_\perp\cdot\left(\frac{1}{\rho}\nabla_\perp\right)$ is the 2-D Laplacian-like operator, defined as,

$$\rho\nabla_\perp\cdot\left(\frac{1}{\rho}\nabla_\perp\right)=\rho\frac{\partial}{\partial x_1}\left(\frac{1}{\rho}\frac{\partial}{\partial x_1}\right)+\rho\frac{\partial}{\partial x_2}\left(\frac{1}{\rho}\frac{\partial}{\partial x_2}\right)\,, \tag{10}$$

with $\boldsymbol{x}_\perp=\left(x_1,x_2\right)$ are the transverse coordinates.

Computing the square root operator $\sqrt{\mathbf{I}+\mathbf{Q}}$ in equation (7) is generally nontrivial. Several methods have been used to approximate the square root operator, among these are: (i) Taylor-series based methods [35], [38], [39] where a first-order approximation of the operator leads to the standard Narrow-Angle Parabolic Equation (NAPE), and (ii) Padé-series based methods [31], [40], of which the family of Padé WAPE (Pa-WAPE) is derived. Further details about these approximations can be found in the appendix and in [41].

The MSEAS-ParEq software implements equation (7) in its NAPE and Pa-WAPE forms using second-order spatial finite volume (FV) schemes and high-order range marching schemes (second-order backward difference, Crank-Nicholson and high-order Runge-Kutta methods are available for the user). The solver also employs efficient techniques allowing for propagation at larger angles and in bigger domains and has been validated on several benchmark cases [41]. Finally, the MSEAS-ParEq software has been tightly integrated with the MSEAS-PE ocean model allowing for simulating the acoustic propagation in realistic ocean environments, as demonstrated in later sections (in this case, the sound speed and density fields in equations (7) are provided as inputs into the MSEAS-ParEq solver by the MSEAS-PE ocean simulations).

D. Broadband Acoustic Modeling

In addition to TL fields, it is common to predict the acoustic signal received at a location $\boldsymbol{x}^*=\left(\boldsymbol{x}_\perp^*,\eta^*\right)$. This can be done using the Fourier Synthesis technique [38], [42]. This technique involves the following steps:

1) By appropriately choosing the time window and sampling frequency based on the source spectrum, a discrete set of frequencies $\omega_1,\cdots,\omega_N$ is constructed.
2) The frequency-domain PE equation (7) (or one of its variants) is solved for each frequency to obtain the set of solutions $\psi\left(\boldsymbol{x}_\perp^*,\eta^*;\omega_1,\cdots,\omega_N\right)$, and the corresponding normalized pressure solutions $p\left(\boldsymbol{x}_\perp^*,\eta^*;\omega_1,\cdots,\omega_N\right)$ using equation (6).
3) The unnormalized pressures $P\left(\boldsymbol{x}_\perp^*,\eta^*;\omega_1,\cdots,\omega_N\right)$ are constructed using the source spectrum as $P\left(\omega\right)=p\left(\omega\right)\hat{S}\left(\omega\right)$.
4) The time-domain pressure solution $p_t\left(\boldsymbol{x}_\perp^*,\eta^*;t\right)$ is then constructed from the frequency domain solutions using the Inverse Fourier Transform (IFT): $p_t\left(\boldsymbol{x}_\perp^*,\eta^*;t\right)=\mathcal{F}^{-1}\left\{P\left(\boldsymbol{x}_\perp^*,\eta^*;\omega\right)\right\}$.

The MSEAS-ParEq software includes an efficient implementation of this Fourier Synthesis technique which constructs an optimal discrete set of frequencies $\omega_1,\cdots,\omega_N$ (with the minimum number of required frequencies), and uses the Fast Fourier Transform (FFT) algorithm to carry out the IFT into the time domain. Furthermore, the MSEAS-ParEq solver also computes the integrated Transmission Loss (iTL) [32], a commonly used quantity of interest, using the time domain solution $p_t\left(\boldsymbol{x}_\perp^*,\eta^*;t\right)$ as

$$\text{iTL}\left(\boldsymbol{x}_\perp^*,\eta^*\right)=-20\log\left(\frac{1}{T}\int_0^T\left|p_t\left(\boldsymbol{x}_\perp^*,\eta^*;t\right)\right|dt\right)\,, \tag{11}$$

where T is the time window of integration.

E. Probabilistic Acoustic Modeling

An alternative approach to modeling the broadband acoustic propagation in terms of discrete frequency runs of the acoustic PE is to adopt a probabilistic approach in which the frequency is treated as a uniformly distributed random variable over the bandwidth of interest. In this case, the acoustic PE becomes a stochastic PDE (SPDE)

$$v(\eta;\xi) \sim \exp(ik_0(\xi)\eta),$$
$$\frac{\partial}{\partial\eta}\psi(\boldsymbol{x}_\perp,\eta;\xi) = ik_0(\xi)\left\{\sqrt{\mathbf{I}+\mathbf{Q}(\xi)}-\mathbf{I}\right\}\psi(\boldsymbol{x}_\perp,\eta;\xi), \quad (12)$$

where $\xi \in \Xi$ denotes the random parameter.
Several methods have been proposed to model the stochastic acoustic propagation, namely Monte Carlo (MC) sampling [43], Error Subspace Statistical Estimation (ESSE) [2], [4], [44], [45], Probability Density Function (PDF) propagation [46], Field Shifting (FS) [47], [48] and Polynomial Chaos (PC) expansion techniques [49], [50]. Yet, most of these methods have only been tested in canonical test cases and can fail to provide sufficiently accurate results (at reasonable computational costs) in realistic ocean applications, which is the case in this work.

In the present simulations, we thus utilize our stochastic propagation modeling approach based on the Dynamically-Orthogonal (DO) equations [51]–[54] to capture the uncertainties using an instantaneously-optimal dynamic reduction, nonlinear governing equations for the DO decomposition, rich non-Gaussian statistics equivalent to large MC ensembles, and at relatively low computational costs [41], [55]. Under this technique the stochastic acoustic field $(\psi(\boldsymbol{x}_\perp,\eta;\xi))$ is represented using a range-evolving DO decomposition,

$$\psi(\boldsymbol{x}_\perp,\eta;\xi) = \bar{\psi}(\boldsymbol{x}_\perp,\eta) + \sum_{i=1}^{n_{s,\psi}} \tilde{\psi}_i(\boldsymbol{x}_\perp,\eta)\,\alpha_i(\eta;\xi), \quad (13)$$

where $\bar{\psi}(\boldsymbol{x}_\perp,\eta)$ is the mean field, and $\tilde{\psi}_i(\boldsymbol{x}_\perp,\eta)$ are orthonormal modes that form an ordered basis for the stochastic subspace of size $n_{s,\psi}$. In addition, $\alpha_i(\eta;\xi)$ are zero-mean stochastic processes.
By substituting this decomposition into the governing SPDEs in equation (12), predictive equations for the (range) evolution of the mean, modes and stochastic coefficients can be derived. Further details about these equations and their numerical implementation can be found in [55] and [41].

III. Results and Discussion

A. Coupled Ocean Physics-Acoustics Simulations

We downscaled initial conditions from HYCOM simulations. Our downscaling scheme used limited independent synoptic data of opportunity and our feature modeling capabilities to correct the coarse HYCOM fields. The effects of these corrections are illustrated in Fig. 4. In the left panel, we compare HYCOM and MSEAS-PE simulated profiles to independent XBT profiles (not utilized in any of the simulations). The higher resolutions from the MSEAS-PE simulations and the corrections from the available synoptic data of opportunity clearly improves the temperature below 30 m. The average RMS error is reduced by a factor of 3 and the average bias reduced by roughly a factor of 50. Looking at the 30 m sound speed map (middle panel) and sound speeds section along the XBT line (right panel), the data corrections and our feature model introduce colder deep water on the shelf near the XBT region and also sharper gradients, both near the front and vertically. Sound speed gradients are similarly enhanced.

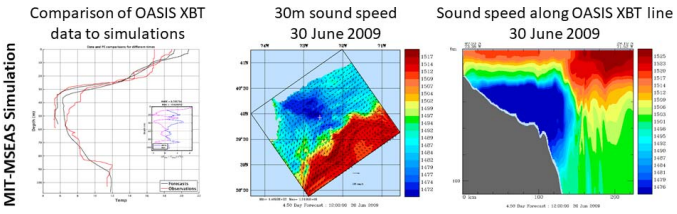

Fig. 4. MIT-MSEAS high resolution simulations using our downscaling scheme which used independent synoptic data of opportunity and our MIT-MSEAS feature modeling capabilities to correct the coarse HYCOM fields.

The effects of tides on sound speed from our MSEAS-PE can also be seen in the middle and right panels of Fig. 4. Between June 29 and July 2, 2009, internal tides move colder water (lower sound speed) up into the mid-level (30m). These internal tides also advect the shelf break front back and forth.

The 30 m scaled vorticity on June 30, 2009, from our MSEAS-PE is shown in Fig. 5. Between June 26 and July 5, sub-mesoscale filaments develop along the shelf break, including southeast of the operational area.

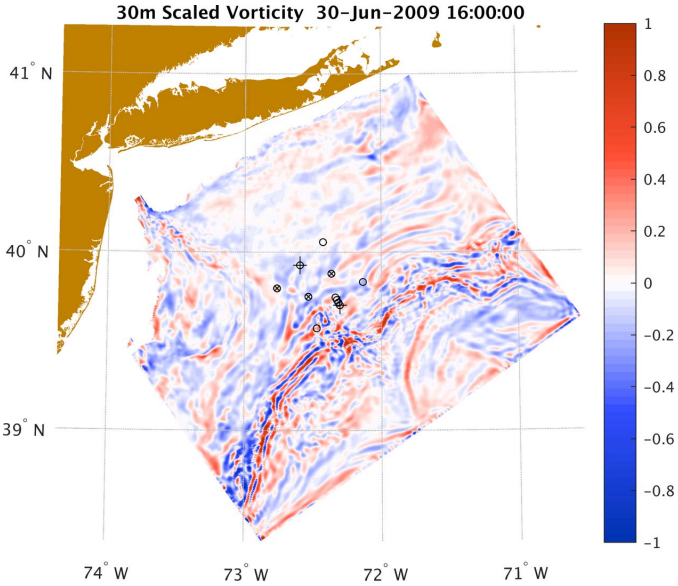

Fig. 5. MSEAS-PE scaled vorticity at 30 m on June 30, 2009. Black crosses denote the OASIS XBT positions; black x's, source positions; black circles, receiver positions.

B. Deterministic Transmission Loss Predictions

The MSEAS-ParEq software was used to predict the transmission loss (TL) fields across 2D sections in the MAC DG-3 test, using the MSEAS ocean fields as inputs. The TL fields were computed for the three sources and nine receivers for different times and different frequencies.

In Figs. 6 and 7, we show the results obtained for only a representative section and for source A at a single time and for the single central frequency. Results for other sections and sources lead to similar results. Fig. 6 shows the source and receiver locations for this test along with the sea surface sound speed forecast from the MSEAS-PE. A contour map of the sound speed across the section from source A to receiver H as predicted by our MSEAS-PE is also shown in Fig. 7.

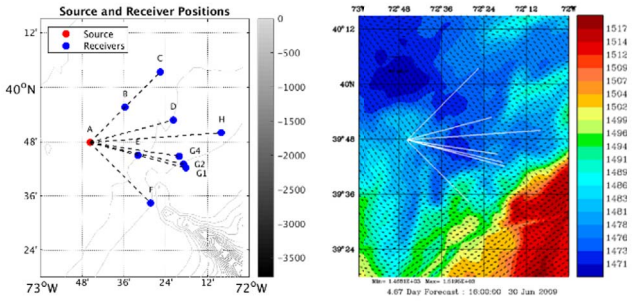

Fig. 6. The distribution of sources and receivers (left) and the sound speed field at the sea surface, from a forecast by our data assimilative MSEAS-PE ocean model, in the region of interest (right).

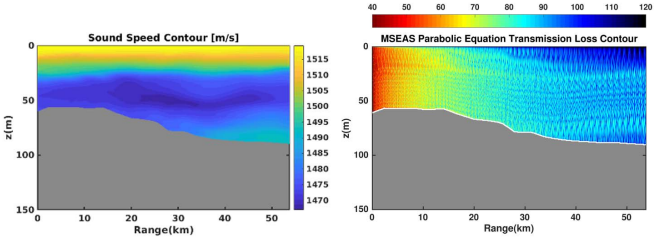

Fig. 7. The forecast sound speed field for the section between the source at location A and the receiver at location H (left). The predicted transmission loss contour from the MSEAS-ParEq solver for section A-H (for a fixed frequency of 950 Hz) (right).

The MSEAS-PE ocean hindcasts of the sound speed fields (computed from the temperature and salinity hindcasts) are then transferred as inputs to the MSEAS-ParEq model to obtain predictions of the transmission loss fields across the section A-H from a time-harmonic source of frequency 950 Hz located at 65 ft ($\approx$ 20 m) depth (Fig. 7). For the acoustic propagation simulations, a grid resolution of 0.5 m in range and depth was used to resolve the small scale features in the acoustic fields. Furthermore, no attenuation was considered in the water.

The seabed is of critical importance for accurate acoustic propagation modeling [36], [56]–[58]. The SW06 area, a region whose seabed has been studied and examined in previous experiments, is relatively complex and has highly variable sedimentary properties. The seabed parameters used in the model were obtained using results from these previous studies [59]–[61]. Due to the relatively high prevalence of clay in the upper layers of the ocean bottom, the seabed in the simplified propagation model was represented homogeneously using solely this material.

C. Stochastic Transmission Loss Predictions

In addition to the deterministic TL predictions presented previously, the MSEAS-ParEq software was used to provide stochastic TL predictions, using the DO acoustics ParEq approach [55]. This was done for the section A-H where the time-harmonic sound source located at 65 ft depth has an uncertain frequency $f \sim U[850, 1050]$ Hz. The DO acoustic ParEq yields the predictions for the mean field, mode fields, and stochastic coefficients, from which classic statistical quantities such as the standard deviation field and other moments can be computed. The DO acoustic ParEq results are illustrated on Fig. 8 where only DO modes 1 and 2 are shown. The stochastic predictions were obtained with $n_{s,\psi} = 50$ and the depth and range resolutions used for the deterministic simulation.

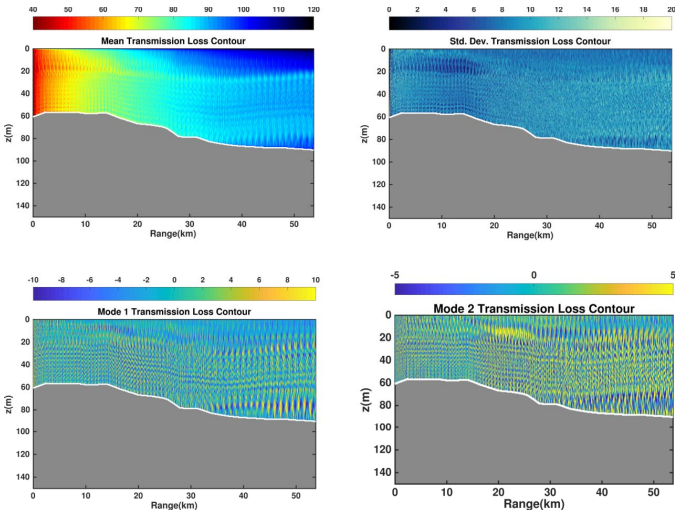

Fig. 8. DO solution for the stochastic TL field in section A-H. The mean, standard deviation, and modes 1 and 2 (out of the 50 modes retained in the truncation) of the TL field are shown.

D. Integrated Transmission Loss Skill

Starting from the single frequency runs obtained from the MSEAS-ParEq solver, the developed broadband techniques were employed to obtain predictions for the integrated transmission loss (iTL) due to a high-frequency modulated (HFM) sound source with central frequency of 950 Hz, a bandwidth of 100 Hz and a 5 seconds pulse width. We also compared these results to measurements obtained from the three sources during the MAC DG-3 test.

In Fig. 9, we show comparisons of the iTL values at the receiver locations due to a HFM sound source located at A,

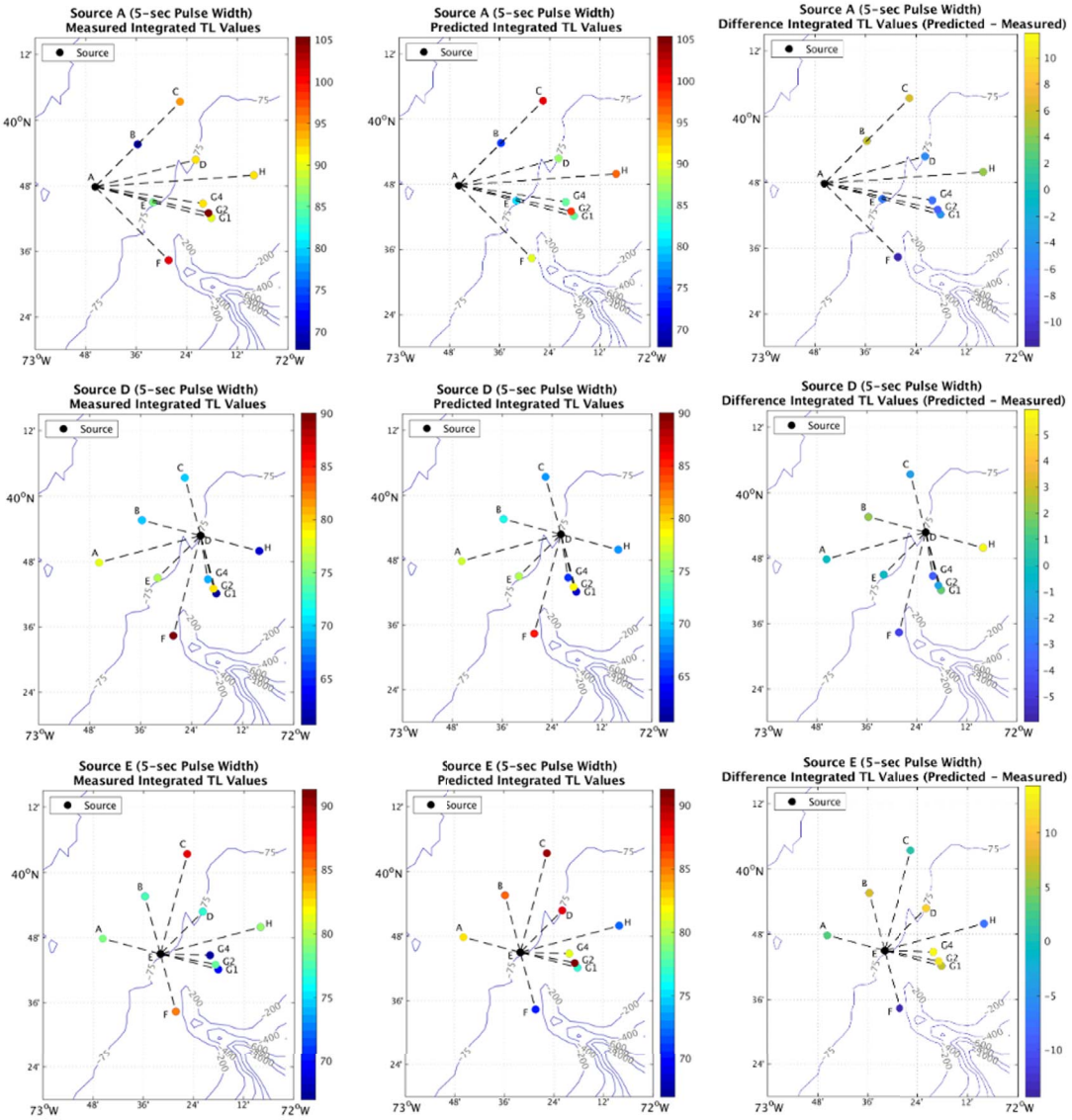

Fig. 9. Predicted and measured integrated transmission loss (iTL) values for the different sources (top row corresponds to source A, middle row to source D and bottom row to source E). The measured integrated TL values at each receiver for each source for a 5 second pulse width (left column). The predicted integrated TL values as obtained from the MSEAS-ParEq solver (middle column). The difference between the predicted and measured values (right column).

D and E. The results for each distinct source is shown in a separate row. Specifically, the left column of sub-figures in Fig. 9 shows points at the receiver locations colored by their corresponding measured iTL values. In the middle column of sub-figures in Fig. 9, the predicted iTL values as obtained by the MSEAS-ParEq solver are shown. The discrepancies between the measured and predicted results are depicted in rightmost column of sub-figures. For each of the three sources, the predicted iTL values are found to match well with the measured data (within 5 dB and smaller mean error). In general, a somewhat larger discrepancy can be noted at the receiver F, located across the shelf break, which can be due to uncertainties in locating the shelf break front, in water properties in the Hudson Canyon, and/or in the seabed and bathymetry.

The above results are further quantified by the histogram shown in Fig. 10. Specifically, Fig. 10 provides the histogram of the aggregated error values at all receivers due to the 3 sources A, D and E. The results show an overall small mean error of 1.102 dB and standard deviation error of 6.239 dB value. These values are within or close to the standard errors of the iTL measurements (not shown). We can note from the histogram results that the mean error is close to zero, providing future opportunities for inferring the source level.

IV. Conclusion

We updated our MIT-MSEAS ocean physics-acoustics modeling system including 3D multi-resolution finite-volume ocean modeling for the MAC DG-3 test region. Our use of independent data to correct downscaled ocean initial-conditions

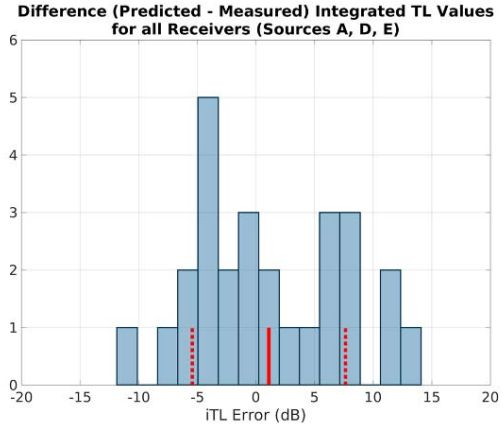

Fig. 10. Histogram of the difference (predicted – measured) integrated transmission loss (iTL) values for all receivers transmitting from the three sources A, D and E. The solid line corresponds to the mean iTL error value (1.102 dB), and the dashed lines around it correspond to 1 standard deviation (6.539 dB).

was shown to reduce ocean RMSE by a factor of 3 and bias by a factor of 50. For the acoustics, we showcased application of our MSEAS-ParEq solver in predicting deterministic and stochastic TL fields in 2D ocean sections for the MAC DG-3 test.

Multiple extensions to the present work are presently ongoing. These include the use of additional nesting and tiling subdomains, finite-element non-hydrostatic ocean simulationsc [62], ESSE for ensemble forecasting [4], [63], Dynamically-Orthogonal PEs for surface ducts, the GMM-DO filter and smoother [64], [65] for ocean-physics-acoustics inversion and tomography, and Bayesian mutual information fields for determining the optimal sampling and measurement locations [66] in future sea tests.

The relatively small discrepancies between the measured and predicted iTL values can be mostly explained by: (i) mismatches between the simulated and actual ocean fields, and (ii) the need for more accurate seabed modeling. An approach to address these challenges is to apply our efficient joint Bayesian inversion of the ocean-physics-acoustics-seabed fields. We are completing such Bayesian inversion using our novel optimally-adaptive dynamically orthogonal (DO) equations and Gaussian mixture model (GMM)-DO smoother and filter [41], [67], [68].

Appendix - Narrow and Wide-Angle PE Approximations

The standard narrow-angle PE (NAPE), which is the most widely used within the acoustics community [35], can be derived as an example of a Taylor-series based PE by retaining one term in the Taylor series approximation of the square root operator,

$$\sqrt{\mathbf{I}+\mathbf{Q}} \approx \mathbf{I} + \frac{1}{2}\mathbf{Q}\,, \tag{14}$$

to obtain,

$$\frac{\partial}{\partial \eta}\psi\left(\boldsymbol{x}_\perp,\eta\right) = \left\{ \frac{ik_0}{2}\left(n_a^2-1\right) + \frac{i}{2k_0}\rho\nabla_\perp\cdot\left(\frac{1}{\rho}\nabla_\perp\right) \right\}\psi\left(\boldsymbol{x}_\perp,\eta\right) \tag{15}$$

The NAPE can be interpreted as a reaction-diffusion PDE. The Taylor-series approximation makes the equation only valid for computing propagation at an angle ± 15 degrees around the source, and hence the name narrow-angle [32], [35].

Padé-series based PE [31] can be alternatively derived by approximating the square root operator using the m-term Padé approximant,

$$\sqrt{\mathbf{I}+\mathbf{Q}} \approx \mathbf{I} + \sum_{j=1}^{m} \frac{a_{j,m}\mathbf{Q}}{\mathbf{I}+b_{j,m}\mathbf{Q}}\,, \tag{16}$$

where the coefficients are given as,

$$a_{j,m} = \frac{2}{2m+1}\sin^2\left(\frac{j\pi}{2m+1}\right), b_{j,m} = \cos^2\left(\frac{j\pi}{2m+1}\right). \tag{17}$$

For instance, $m=1$ corresponds to the Claerbout WAPE [40] with ± 55 degrees propagation angle. The Padé WAPE (Pa-WAPE) then correspond to the following PDE form,

$$\frac{\partial}{\partial \eta}\psi\left(\boldsymbol{x}_\perp,\eta\right) = \left\{ ik_0 \sum_{j=1}^{m} \left(\mathbf{I}+b_{j,m}\mathbf{Q}\right)^{-1} a_{j,m}\mathbf{Q} \right\}\psi\left(\mathbf{x}_\perp,\eta\right). \tag{18}$$

The different families of approximants have been summarized in [69].

Acknowledgments

We thank all members of the MSEAS group, past and present. We are grateful to NAVAIR for support under grant N18A-002-0056 (STTR S-DUCT). We thank the HYCOM team for their ocean fields, NMFS (Tamara Holzwarth-Davis and Paula Fratantoni) for their survey CTD data, NCEP (Matthew Pyle, Eric Rogers, Geoff DiMego, and Arun Chawla) for their help and support for atmospheric forcing forecasts, NOAA NDBC for supplying buoy data, and JHU APL for processed SST images.

References

[1] A. R. Robinson, P. Abbot, P. F. J. Lermusiaux, and L. Dillman, "Transfer of uncertainties through physical-acoustical-sonar end-to-end systems: A conceptual basis," in *Acoustic Variability, 2002*, N. G. Pace and F. B. Jensen, Eds. SACLANTCEN, Kluwer Academic Press, 2002, pp. 603–610.

[2] A. R. Robinson and P. F. J. Lermusiaux, "Prediction systems with data assimilation for coupled ocean science and ocean acoustics," in *Proceedings of the Sixth International Conference on Theoretical and Computational Acoustics*, A. Tolstoy et al, Ed. World Scientific Publishing, 2004, pp. 325–342, refereed invited Keynote Manuscript.

[3] P. F. J. Lermusiaux, C.-S. Chiu, G. G. Gawarkiewicz, P. Abbot, A. R. Robinson, R. N. Miller, P. J. Haley, Jr, W. G. Leslie, S. J. Majumdar, A. Pang, and F. Lekien, "Quantifying uncertainties in ocean predictions," *Oceanography*, vol. 19, no. 1, pp. 92–105, 2006.

[4] P. F. J. Lermusiaux, J. Xu, C.-F. Chen, S. Jan, L. Chiu, and Y.-J. Yang, "Coupled ocean–acoustic prediction of transmission loss in a continental shelfbreak region: Predictive skill, uncertainty quantification, and dynamical sensitivities," *IEEE Journal of Oceanic Engineering*, vol. 35, no. 4, pp. 895–916, Oct. 2010.

[5] T. F. Duda, Y.-T. Lin, A. E. Newhall, K. R. Helfrich, J. F. Lynch, W. G. Zhang, P. F. J. Lermusiaux, and J. Wilkin, "Multiscale multiphysics data-informed modeling for three-dimensional ocean acoustic simulation and prediction," *Journal of the Acoustical Society of America*, vol. 146, no. 3, pp. 1996–2015, Sep. 2019.

[6] P. J. Haley, Jr. and P. F. J. Lermusiaux, "Multiscale two-way embedding schemes for free-surface primitive equations in the "Multidisciplinary Simulation, Estimation and Assimilation System"," *Ocean Dynamics*, vol. 60, no. 6, pp. 1497–1537, Dec. 2010.

[7] MSEAS Group, "MSEAS Software," 2013. [Online]. Available: http://mseas.mit.edu/software/

[8] P. J. Haley, Jr., A. Agarwal, and P. F. J. Lermusiaux, "Optimizing velocities and transports for complex coastal regions and archipelagos," *Ocean Modeling*, vol. 89, pp. 1–28, 2015.

[9] W. G. Leslie, A. R. Robinson, P. J. Haley, Jr, O. Logutov, P. A. Moreno, P. F. J. Lermusiaux, and E. Coelho, "Verification and training of real-time forecasting of multi-scale ocean dynamics for maritime rapid environmental assessment," *Journal of Marine Systems*, vol. 69, no. 1, pp. 3–16, 2008.

[10] R. Onken, A. Álvarez, V. Fernández, G. Vizoso, G. Basterretxea, J. Tintoré, P. Haley, Jr., and E. Nacini, "A forecast experiment in the Balearic Sea." *Journal of Marine Systems*, vol. 71, no. 1-2, pp. 79–98, 2008.

[11] P. J. Haley, Jr., P. F. J. Lermusiaux, A. R. Robinson, W. G. Leslie, O. Logoutov, G. Cossarini, X. S. Liang, P. Moreno, S. R. Ramp, J. D. Doyle, J. Bellingham, F. Chavez, and S. Johnston, "Forecasting and reanalysis in the Monterey Bay/California Current region for the Autonomous Ocean Sampling Network-II experiment," *Deep Sea Research Part II: Topical Studies in Oceanography*, vol. 56, no. 3–5, pp. 127–148, Feb. 2009.

[12] A. Gangopadhyay, P. F. Lermusiaux, L. Rosenfeld, A. R. Robinson, L. Calado, H. S. Kim, W. G. Leslie, and P. J. Haley, Jr., "The California Current system: A multiscale overview and the development of a feature-oriented regional modeling system (FORMS)," *Dynamics of Atmospheres and Oceans*, vol. 52, no. 1–2, pp. 131–169, Sep. 2011, Special issue of Dynamics of Atmospheres and Oceans in honor of Prof. A. R. Robinson.

[13] S. R. Ramp, P. F. J. Lermusiaux, I. Shulman, Y. Chao, R. E. Wolf, and F. L. Bahr, "Oceanographic and atmospheric conditions on the continental shelf north of the Monterey Bay during August 2006," *Dynamics of Atmospheres and Oceans*, vol. 52, no. 1–2, pp. 192–223, Sep. 2011, Special issue of Dynamics of Atmospheres and Oceans in honor of Prof. A. R. Robinson.

[14] M. E. G. D. Colin, T. F. Duda, L. A. te Raa, T. van Zon, P. J. Haley, Jr., P. F. J. Lermusiaux, W. G. Leslie, C. Mirabito, F. P. A. Lam, A. E. Newhall, Y.-T. Lin, and J. F. Lynch, "Time-evolving acoustic propagation modeling in a complex ocean environment," in *OCEANS - Bergen, 2013 MTS/IEEE*, 2013, pp. 1–9.

[15] P. F. J. Lermusiaux, P. J. Haley, Jr., S. Jana, A. Gupta, C. S. Kulkarni, C. Mirabito, W. H. Ali, D. N. Subramani, A. Dutt, J. Lin, A. Shcherbina, C. Lee, and A. Gangopadhyay, "Optimal planning and sampling predictions for autonomous and Lagrangian platforms and sensors in the northern Arabian Sea," *Oceanography*, vol. 30, no. 2, pp. 172–185, Jun. 2017, special issue on Autonomous and Lagrangian Platforms and Sensors (ALPS).

[16] D. N. Subramani, P. F. J. Lermusiaux, P. J. Haley, Jr., C. Mirabito, S. Jana, C. S. Kulkarni, A. Girard, D. Wickman, J. Edwards, and J. Smith, "Time-optimal path planning: Real-time sea exercises," in *Oceans '17 MTS/IEEE Conference*, Aberdeen, Jun. 2017.

[17] C. S. Kulkarni, P. J. Haley, Jr., P. F. J. Lermusiaux, A. Dutt, A. Gupta, C. Mirabito, D. N. Subramani, S. Jana, W. H. Ali, T. Peacock, C. M. Royo, A. Rzeznik, and R. Supekar, "Real-time sediment plume modeling in the Southern California Bight," in *OCEANS Conference 2018*. Charleston, SC: IEEE, Oct. 2018.

[18] A. Gupta, P. J. Haley, D. N. Subramani, and P. F. J. Lermusiaux, "Fish modeling and Bayesian learning for the Lakshadweep Islands," in *OCEANS 2019 MTS/IEEE SEATTLE*. Seattle: IEEE, Oct. 2019, pp. 1–10.

[19] P. F. J. Lermusiaux, M. Doshi, C. S. Kulkarni, A. Gupta, P. J. Haley, Jr., C. Mirabito, F. Trotta, S. J. Levang, G. R. Flierl, J. Marshall, T. Peacock, and C. Noble, "Plastic pollution in the coastal oceans: Characterization and modeling," in *OCEANS 2019 MTS/IEEE SEATTLE*. Seattle: IEEE, Oct. 2019, pp. 1–10.

[20] P. F. J. Lermusiaux, P. J. Haley, Jr, and N. K. Yilmaz, "Environmental prediction, path planning and adaptive sampling: sensing and modeling for efficient ocean monitoring, management and pollution control," *Sea Technology*, vol. 48, no. 9, pp. 35–38, 2007.

[21] Ş. T. Beşiktepe, P. F. J. Lermusiaux, and A. R. Robinson, "Coupled physical and biogeochemical data-driven simulations of Massachusetts Bay in late summer: Real-time and post-cruise data assimilation," *Journal of Marine Systems*, vol. 40–41, pp. 171–212, 2003.

[22] G. Cossarini, P. F. J. Lermusiaux, and C. Solidoro, "Lagoon of Venice ecosystem: Seasonal dynamics and environmental guidance with uncertainty analyses and error subspace data assimilation," *Journal of Geophysical Research: Oceans*, vol. 114, no. C6, Jun. 2009.

[23] P. F. J. Lermusiaux, "On the mapping of multivariate geophysical fields: Sensitivities to size, scales, and dynamics," *Journal of Atmospheric and Oceanic Technology*, vol. 19, no. 10, pp. 1602–1637, 2002.

[24] J. Xu, P. F. J. Lermusiaux, P. J. Haley Jr., W. G. Leslie, and O. G. Logutov, "Spatial and Temporal Variations in Acoustic propagation during the PLUSNet-07 Exercise in Dabob Bay," in *Proceedings of Meetings on Acoustics (POMA)*, vol. 4. Acoustical Society of America 155th Meeting, 2008, p. 11.

[25] F.-P. A. Lam, P. J. Haley, Jr., J. Janmaat, P. F. J. Lermusiaux, W. G. Leslie, M. W. Schouten, L. A. te Raa, and M. Rixen, "At-sea real-time coupled four-dimensional oceanographic and acoustic forecasts during Battlespace Preparation 2007," *Journal of Marine Systems*, vol. 78, no. Supplement, pp. S306–S320, Nov. 2009.

[26] T. F. Duda, Y.-T. Lin, W. Zhang, B. D. Cornuelle, and P. F. J. Lermusiaux, "Computational studies of three-dimensional ocean sound fields in areas of complex seafloor topography and active ocean dynamics," in *Proceedings of the 10th International Conference on Theoretical and Computational Acoustics*, Taipei, Taiwan, 2011.

[27] National Centers for Environmental Information (NCEI), "Coastal Relief Model," 2018. [Online]. Available: https://www.ngdc.noaa.gov/mgg/coastal/crm.html

[28] National Centers for Environmental Prediction (NCEP), "North American Model," 2018. [Online]. Available: https://www.ncdc.noaa.gov/data-access/model-data/model-datasets/north-american-mesoscale-forecast-system-nam

[29] G. D. Egbert and S. Y. Erofeeva, "Efficient inverse modeling of barotropic ocean tides." *Journal of Atmospheric and Oceanic Technology*, vol. 19, no. 2, pp. 183–204, 2002.

[30] ——, "TPXO8-ATLAS," 2013, oSU. [Online]. Available: http://volkov.oce.orst.edu/tides/tpxo8_atlas.html

[31] F. Sturm and J. A. Fawcett, "On the use of higher-order azimuthal schemes in 3-d pe modeling," *JASA*, vol. 113, no. 6, pp. 3134–3145, 2003.

[32] F. B. Jensen, W. A. Kuperman, M. B. Porter, and H. Schmidt, *Computational ocean acoustics*. Springer Science & Business Media, 2011.

[33] Y.-T. Lin, T. F. Duda, and A. E. Newhall, "Three-dimensional sound propagation models using the parabolic-equation approximation and the split-step fourier method," *J. of Computational Acoustics*, vol. 21, no. 01, p. 1250018, 2013.

[34] L. M. Brekhovskikh and O. A. Godin, *Acoustics of layered media II: point sources and bounded beams*. Springer Science & Business Media, 2013, vol. 10.

[35] F. D. Tappert, "The parabolic approximation method," in *Wave Propagation and Underwater Acoustics*, ser. Lecture Notes in Physics, Berlin Springer Verlag, J. B. Keller and J. S. Papadakis, Eds., vol. 70, 1977, p. 224.

[36] P. C. Etter, *Underwater acoustic modeling and simulation*. CRC press, 2018.

[37] Y.-T. Lin, T. F. Duda, and A. E. Newhall, "Three-dimensional sound propagation models using the parabolic-equation approximation and the split-step fourier method," *J. of Computational Acoustics*, vol. 21, no. 01, p. 1250018, 2013. [Online]. Available: http://www.worldscientific.com/doi/abs/10.1142/S0218396X1250018X

[38] F. Sturm, "Numerical study of broadband sound pulse propagation in three-dimensional oceanic waveguides," *JASA*, vol. 117, no. 3, pp. 1058–1079, 2005.

[39] Y.-T. Lin, J. M. Collis, and T. F. Duda, "A three-dimensional parabolic equation model of sound propagation using higher-order operator splitting and padé approximants," *JASA*, vol. 132, no. 5, pp. EL364–EL370, 2012.

[40] J. F. Claerbout, *Fundamentals of geophysical data processing*. Citeseer, 1985.

[41] W. H. Ali, M. S. Bhabra, P. F. J. Lermusiaux, A. March, J. R. Edwards, K. Rimpau, and P. Ryu, "Stochastic oceanographic-acoustic prediction

and Bayesian inversion for wide area ocean floor mapping," in *OCEANS 2019 MTS/IEEE SEATTLE*. Seattle: IEEE, Oct. 2019, pp. 1–10.

[42] F. Tappert, J. L. Spiesberger, and L. Boden, "New full-wave approximation for ocean acoustic travel time predictions," *The Journal of the Acoustical Society of America*, vol. 97, no. 5, pp. 2771–2782, 1995. [Online]. Available: https://doi.org/10.1121/1.411908

[43] P. Gerstoft and C. F. Mecklenbräuker, "Ocean acoustic inversion with estimation of a posteriori probability distributions," *J. of the Acoustical Society of America*, vol. 104, no. 2, pp. 808–819, 1998.

[44] P. F. J. Lermusiaux, C.-S. Chiu, and A. R. Robinson, "Modeling uncertainties in the prediction of the acoustic wavefield in a shelfbreak environment," in *Proceedings of the 5th International conference on theoretical and computational acoustics*, E.-C. Shang, Q. Li, and T. F. Gao, Eds. World Scientific Publishing Co., May 21-25 2002, pp. 191–200, refereed invited manuscript.

[45] P. F. J. Lermusiaux, "Uncertainty estimation and prediction for interdisciplinary ocean dynamics," *Journal of Computational Physics*, vol. 217, no. 1, pp. 176–199, 2006.

[46] K. R. James and D. R. Dowling, "A probability density function method for acoustic field uncertainty analysis," *J. of the Acoustical Society of America*, vol. 118, no. 5, pp. 2802–2810, 2005.

[47] S. E. Dosso, M. G. Morley, P. M. Giles, G. H. Brooke, D. F. McCammon, S. Pecknold, and P. C. Hines, "Spatial field shifts in ocean acoustic environmental sensitivity analysis," *J. of the Acoustical Society of America*, vol. 122, no. 5, pp. 2560–2570, 2007.

[48] K. R. James and D. R. Dowling, "A method for approximating acoustic-field-amplitude uncertainty caused by environmental uncertainties," *J. of the Acoustical Society of America*, vol. 124, no. 3, pp. 1465–1476, 2008.

[49] Y. Y. Khine, D. B. Creamer, and S. Finette, "Acoustic propagation in an uncertain waveguide environment using stochastic basis expansions," *Journal of Computational Acoustics*, vol. 18, no. 04, pp. 397–441, 2010.

[50] S. Finette, "A stochastic representation of environmental uncertainty and its coupling to acoustic wave propagation in ocean waveguides," *J. of the Acoustical Society of America*, vol. 120, no. 5, pp. 2567–2579, 2006.

[51] T. P. Sapsis and P. F. J. Lermusiaux, "Dynamically orthogonal field equations for continuous stochastic dynamical systems," *Physica D: Nonlinear Phenomena*, vol. 238, no. 23–24, pp. 2347–2360, Dec. 2009.

[52] ——, "Dynamical criteria for the evolution of the stochastic dimensionality in flows with uncertainty," *Physica D: Nonlinear Phenomena*, vol. 241, no. 1, pp. 60–76, 2012.

[53] M. P. Ueckermann, P. F. J. Lermusiaux, and T. P. Sapsis, "Numerical schemes for dynamically orthogonal equations of stochastic fluid and ocean flows," *Journal of Computational Physics*, vol. 233, pp. 272–294, Jan. 2013.

[54] F. Feppon and P. F. J. Lermusiaux, "A geometric approach to dynamical model-order reduction," *SIAM Journal on Matrix Analysis and Applications*, vol. 39, no. 1, pp. 510–538, 2018.

[55] W. H. Ali, "Dynamically orthogonal equations for stochastic underwater sound propagation," Master's thesis, Massachusetts Institute of Technology, Computation for Design and Optimization Program, Cambridge, Massachusetts, Sep. 2019.

[56] E. L. Hamilton, "Geoacoustic modeling of the sea floor," *The Journal of the Acoustical Society of America*, vol. 68, no. 5, pp. 1313–1340, 1980.

[57] M. J. Buckingham, "Ocean-acoustic propagation models," *J. Acoustique*, pp. 223–287, 1992.

[58] L. Bjørnø, *Applied underwater acoustics*. Elsevier, 2017.

[59] D. Tang, J. N. Moum, J. F. Lynch, P. Abbot, R. Chapman, P. H. Dahl, T. F. Duda, G. Gawarkiewicz, S. Glenn, J. A. Goff *et al.*, "Shallow water'06: A joint acoustic propagation/nonlinear internal wave physics experiment," *Oceanography*, vol. 20, no. 4, pp. 156–167, 2007.

[60] M. S. Ballard, K. M. Becker, and J. A. Goff, "Geoacoustic inversion for the new jersey shelf: 3-d sediment model," *IEEE Journal of Oceanic Engineering*, vol. 35, no. 1, pp. 28–42, 2010.

[61] J. A. Goff, "Stratigraphic and geoacoustic characterization of the outer new jersey shelf," TEXAS UNIV AT AUSTIN INST FOR GEOPHYSICS, Tech. Rep., 2010.

[62] M. P. Ueckermann and P. F. J. Lermusiaux, "Hybridizable discontinuous Galerkin projection methods for Navier–Stokes and Boussinesq equations," *Journal of Computational Physics*, vol. 306, pp. 390–421, 2016.

[63] P. F. J. Lermusiaux, C. Mirabito, P. J. Haley, Jr., W. H. Ali, A. Gupta, S. Jana, E. Dorfman, A. Laferriere, A. Kofford, G. Shepard, M. Goldsmith, K. Heaney, E. Coelho, J. Boyle, J. Murray, L. Freitag, and A. Morozov, "Real-time probabilistic coupled ocean physics-acoustics forecasting and data assimilation for underwater GPS," in *OCEANS 2020 IEEE/MTS*. IEEE, Oct. 2020, in press.

[64] T. Sondergaard and P. F. J. Lermusiaux, "Data assimilation with Gaussian Mixture Models using the Dynamically Orthogonal field equations. Part I: Theory and scheme." *Monthly Weather Review*, vol. 141, no. 6, pp. 1737–1760, 2013.

[65] T. Lolla and P. F. J. Lermusiaux, "A Gaussian mixture model smoother for continuous nonlinear stochastic dynamical systems: Theory and scheme," *Monthly Weather Review*, vol. 145, pp. 2743–2761, Jul. 2017.

[66] P. F. J. Lermusiaux, D. N. Subramani, J. Lin, C. S. Kulkarni, A. Gupta, A. Dutt, T. Lolla, P. J. Haley, Jr., W. H. Ali, C. Mirabito, and S. Jana, "A future for intelligent autonomous ocean observing systems," *Journal of Marine Research*, vol. 75, no. 6, pp. 765–813, Nov. 2017, the Sea. Volume 17, The Science of Ocean Prediction, Part 2.

[67] T. Sondergaard and P. F. J. Lermusiaux, "Data assimilation with Gaussian Mixture Models using the Dynamically Orthogonal field equations. Part II: Applications." *Monthly Weather Review*, vol. 141, no. 6, pp. 1761–1785, 2013.

[68] T. Lolla and P. F. J. Lermusiaux, "A Gaussian mixture model smoother for continuous nonlinear stochastic dynamical systems: Applications," *Monthly Weather Review*, vol. 145, pp. 2763–2790, Jul. 2017.

[69] L. Halpern and L. N. Trefethen, "Wide-angle one-way wave equations," *The Journal of the Acoustical Society of America*, vol. 84, no. 4, pp. 1397–1404, 1988. [Online]. Available: https://doi.org/10.1121/1.396586